Artificial Intelligence in Geosciences 2 (2021) 35–46

Contents lists available at ScienceDirect

Artificial Intelligence in Geosciences

journal homepage: www.keaipublishing.com/en/journals/artificial-intelligence-in-geosciences

Near-surface velocity inversion from Rayleigh wave dispersion curves based on a differential evolution simulated annealing algorithm

Yaojun Wang [a], Hua Wang [a,*], Xijun Wu [a], Keyu Chen [a], Sheng Liu [b], Xiaodong Deng [b]

[a] Center for Information Geoscience, University of Electronic Science and Technology of China, Chengdu, 5162125, China
[b] South Branch of Sinopec Geophysical Corporation, Chengdu, 610041, China

ARTICLE INFO

Keywords:
Simulated annealing
Differential evolution
Block coordinate descent
Surface wave dispersion curve
Nonlinear inversion

ABSTRACT

The utilization of urban underground space in a smart city requires an accurate understanding of the underground structure. As an effective technique, Rayleigh wave exploration can accurately obtain information on the subsurface. In particular, Rayleigh wave dispersion curves can be used to determine the near-surface shear-wave velocity structure. This is a typical multiparameter, high-dimensional nonlinear inverse problem because the velocities and thickness of each layer must be inverted simultaneously. Nonlinear methods such as simulated annealing (SA) are commonly used to solve this inverse problem. However, SA controls the iterative process though temperature rather than the error, and the search direction is random; hence, SA always falls into a local optimum when the temperature setting is inaccurate. Specifically, for the inversion of Rayleigh wave dispersion curves, the inversion accuracy will decrease with an increasing number of layers due to the greater number of inversion parameters and large dimension. To solve the above problems, we convert the multiparameter, high-dimensional inverse problem into multiple low-dimensional optimizations to improve the algorithm accuracy by incorporating the principle of block coordinate descent (BCD) into SA. Then, we convert the temperature control conditions in the original SA method into error control conditions. At the same time, we introduce the differential evolution (DE) method to ensure that the iterative error steadily decreases by correcting the iterative error direction in each iteration. Finally, the inversion stability is improved, and the proposed inversion method, the block coordinate descent differential evolution simulated annealing (BCDESA) algorithm, is implemented. The performance of BCDESA is validated by using both synthetic data and field data from western China. The results show that the BCDESA algorithm has stronger global optimization capabilities than SA, and the inversion results have higher stability and accuracy. In addition, synthetic data analysis also shows that BCDESA can avoid the problems of the conventional SA method, which assumes the S-wave velocity structure in advance. The robustness and adaptability of the algorithm are improved, and more accurate shear-wave velocity and thickness information can be extracted from Rayleigh wave dispersion curves.

1. Introduction

With the acceleration of urbanization and with rapid increases in population and economic activity, the utilization of urban underground space (UUS) has become a dramatic strategy in smart cities, which are characterized by massive constructions such as subways, pipeline networks, groundwater projects, and underground malls. UUS utilization requires accurate and efficient measurements of the subsurface. Therefore, efficient measurement methods for determining the extents of near-surface underground structures have become a popular issue in the fields of geophysics and geotechnical engineering.

Existing near-surface survey methods include the high-density electrical method, ground-penetrating radar, reflection seismology, and multichannel analysis of surface waves (MASW) (Xia et al., 1999; Park et al., 1999). Among them, the high-density electrical method and ground-penetrating radar obtain the resistivity distribution of the subsurface, whereas reflection seismology and multichannel transient surface wave methods use the propagation of elastic waves to obtain velocity information and describe the underground structure. The former has a high detection accuracy, but the depth of investigation is limited by the frequency of electromagnetic waves; in contrast, the latter has a high resolution and large investigation depth. In particular, the MASW

* Corresponding author.
E-mail addresses: yaojun.wang@uestc.edu.cn (Y. Wang), huawang@uestc.edu.cn (H. Wang), wuserry@163.com (X. Wu), chloe.chen@std.uestc.edu.cn (K. Chen), shengliu@sinopec.com.cn (S. Liu), dengxd05@hotmail.com (X. Deng).

https://doi.org/10.1016/j.aiig.2021.10.001
Received 15 June 2021; Received in revised form 30 September 2021; Accepted 24 October 2021
Available online 27 October 2021

method, a nondestructive method with a rapid detection speed (Qi et al., 2002) that extracts the dispersion curves of surface waves and then inverts the near-surface velocity information (Xia et al., 1999; Park et al., 1999), is widely used in the detection of UUS (Pugin et al., 2013; Xia et al., 2015).

Surface waves include Rayleigh waves, Love waves, and Stoneley waves; Rayleigh waves, which are formed by P- and SV-waves propagating along the free interface, are the most common. Rayleigh waves become dispersive when the formation depth and velocity vary. Thus, the dispersion curves of Rayleigh waves can be used to invert for the velocity (especially the S-wave velocity, Vs) and thickness of underground media. Although this method is extensively used to image near-surface and deeper earth structures (Zhang et al., 2014; Foti et al., 2011), there are still some challenges, such as the extraction of dispersion curves from surface waves (Zhang et al., 2014) and the acquisition of stable and reliable dispersion curves from an inversion algorithm (Foti et al., 2011; Park et al., 1999). This study will focus on the development of a dispersion curve inversion method.

Numerous inversion methods, both linear and nonlinear, have been used to extract the velocity structure from Rayleigh wave dispersion curves. Linear inversion methods are popular in field applications because of their fast convergence speed. The dispersion equations are linearized, and the inversion results are obtained after the model parameters are modified by a Jacobian matrix. The damped least squares (DLS) and least squares (LM) methods are common linear methods. However, the depth of investigation in field applications typically involves multiple layers (usually more than 3) with the Rayleigh wave method, and the nonlinear problem of inverting multiple parameters (the thickness and velocity in each layer) strongly relies on the initial model, leading to a result with low accuracy and a local optimum solution (Dal Moro et al., 2007). In contrast, nonlinear inversion methods are independent of the initial model and obtain results through a global search; consequently, local extrema are avoided (Lu et al., 2016). The simulated annealing (SA) algorithm (Kirkpatrick et al., 1983) and its derivatives are common nonlinear techniques that are often used for the inversion of Rayleigh wave dispersion curves (e.g., Beaty et al., 2002; Ryden and Park, 2006; Pei et al., 2007; Lu et al., 2016), but these algorithms still have various problems that affect the stability and uniqueness of the inversion:

(1) Dispersion curve inversion requires the simultaneous inversion of multiple sets of layer thicknesses (h) and Vs. The inversion therefore exhibits multiparameter and high-dimensional features, but the conventional SA algorithm adapts poorly to multiparameter, high-dimensional optimization problems (Pei et al., 2008).
(2) The iteration direction in the SA algorithm is random, and the convergence is controlled through temperature; thus, the result may fall into a local optimum due to the limitation on the number of iterations and an inaccurate temperature control.

Accordingly, we propose an improved SA dispersion curve inversion algorithm to address these limitations in two ways:

1) We introduce the block coordinate descending (BCD) method (Zhao et al., 2015; Xu and Yin, 2015) to improve the capability of the SA algorithm to synchronously optimize multiple parameters. Then, the multiple parameters, namely, h and Vs for each layer in a multilayered model, can be inverted by the improved SA algorithm.
2) We introduce the differential evolution (DE) algorithm (Storn and Price, 1997) to control the optimization direction and use the error as the control condition. Thus, the inversion avoids falling into local optima.

Finally, the block coordinate descent differential evolution simulated annealing (BCDESA) algorithm is formed. The new algorithm is verified by synthetic geological models and field data.

2. Method

As described in the introduction, using the SA algorithm to invert the velocities from Rayleigh wave dispersion curves results in a highly nonlinear ill-posed problem. There are two challenges: multiparameter inversion and avoiding locally optimal results. When solving multiparameter problems, the SA algorithm has poor performance (Pei et al., 2008). However, in field applications, we always need to obtain more than 3 parameters to account for all necessary formation layers, and hence, SA is not suitable. The fact that the results obtained by the SA algorithm are locally optimal is a recognized weakness of this technique because the overall iterative process is controlled by temperature and the search direction is random.

2.1. Principle of the velocity inversion from Rayleigh wave dispersion curves

In the inversion of Rayleigh wave dispersion curves, the objective function of the inversion procedure is constructed by the mean square error between the forward model and the observed Rayleigh wave dispersion curve, as shown in equation (1):

$$E = \sqrt{\frac{1}{N}\sum_{i=1}^{N}\left(Vr_i^{obs} - Vr_i^{cal}\right)^2} \tag{1}$$

where N is the number of sampling points on the dispersion curve and Vr_i^{obs} and Vr_i^{cal} are the observed and calculated phase velocities, respectively, at the i^{th} sampling point of the frequency. Here, we can use the generalized reflection-transmission coefficient method (Chen, 1993; Pei et al., 2008) or some other algorithm to calculate the synthetic dispersion curves by using various *Vs*, P-wave velocities (*Vp*), densities (ρ), and *h*. Moreover, the observed curves can be extracted from the *f-k* spectrum of the field Rayleigh wave data.

According to Xia et al. (1999), the influences of *Vp* and ρ on the Rayleigh wave dispersion curve can be ignored. Therefore, we fix *Vp* and ρ during the inversion and invert only *Vs* and *h* to reduce the uncertainty of the inversion. Global optimization algorithms such as SA are usually employed to solve nonlinear objective functions such as equation (1). We introduce the basic principles of the SA in the following section.

2.2. Simulated annealing (SA)

Using the SA algorithm to invert velocity profiles from Rayleigh wave dispersion curves, the model *Vs* and h are perturbed by equation (2):

$$Vs_{i+1}^{j} = Vs_i^j + a^j(V_2 - V_1) and h_{i+1}^j = h_i^j + b^j(H_2 - H_1) \tag{2}$$

where Vs_i^j and Vs_i^{j+1} are the *Vs* values at the i^{th} and $(i+1)^{th}$ iterationsof the j^{th} layer, respectively; h_i^j and h_{i+1}^j are the thicknesses of the i^{th} and $(i+1)^{th}$ iterationsof the j^{th} layer, respectively; (V_1,V_2) represents the *Vs* range of the j^{th} layer; (H_1,H_2) represents the *h* range of the j^{th} layer. Only the parameters in their value ranges are effective in the inversion. The perturbation coefficients *a* and *b* are subjected to a probability distribution, such as a uniform distribution (Beaty et al., 2002) or a Gaussian distribution (Pei et al., 2007). In this paper, we use the coefficients derived from the very fast simulated annealing (VFSA) algorithm (see equation (3)). The advantage of this approach is that the perturbation range of the model becomes narrow when the temperature is decreasing (Ingber, 1989):

$$a, b = \mathrm{sgn}\left(u - \frac{1}{2}\right) T\left[\left(1 + 1/T\right)^{|2u-1|} - 1\right] \tag{3}$$

where sgn is a step function, *u* is subject to a uniform distribution, and *T* is the current temperature.

At the beginning of the inversion, the synthetic dispersion curve is obtained from an initial model (*Vp*, *Vs*, ρ, *h*), and the objective function $\boldsymbol{E_0}$ is calculated using equation (1). Then, at a fixed temperature $\boldsymbol{T}$, we perturb the initial model using equation (2). An updated objective function $\boldsymbol{E_1}$ is calculated, and the variation in the objective function ($\Delta E = \boldsymbol{E_1} - \boldsymbol{E_0}$) is obtained. If ΔE is negative, the new model is accepted; otherwise, the model continues to update. This process is repeated until the iteration meets certain conditions. Next, the value of *T* decreases, and the above process is repeated at the current *T* until a steady state is reached. At this time, the updated model is the output result.

In this paper, the temperature-dropping rule is expressed as

$$T_{k+1} = T_k \alpha^{\sqrt{k}} \tag{4}$$

where *k* is the temperature-dropping number and α is the temperature drop coefficient in the range of [0.8, 0.99] (Pei et al., 2008). This formula is derived from the VFSA method (Ingber, 1989).

After the values of *Vs* and h are updated, *Vp* can be updated according to Poisson's ratio σ and *Vs* (Xia et al., 1999):

$$Vp = Vs\sqrt{\frac{2(1-\sigma)}{1-2\sigma}} \tag{5}$$

ρ is usually a constant, but we can change it depending on the lithology roughly identified from the inverted *Vs* profile.

2.3. Block coordinate descent simulated annealing (BCDSA)

Although the inverted parameters are reduced after considering ρ and *Vp*, in existing Rayleigh wave inversion methods, the parameter dimension is still 2n (n is the number of layers). If n is large, the SA algorithm has difficulty obtaining the ideal outcome (Pei et al., 2008). To avoid the problem of multiple parameters, an alternative iteration approach is proposed. In this scheme, we first disturb *Vs* with a fixed *h* until *Vs* is accepted. Then, *h* is iterated with the updated *Vs* (fixed) until *h* is accepted. If n is large (e.g., n > 3), the iteration errors in each layer will accumulate, and eventually, the inversion will deteriorate.

Here, we use the BCD method (Zhao et al., 2015; Xu and Yin, 2015) to divide the high-dimensional parameter problem into multiple one-dimensional local iterative optimization problems. In each iteration, we first update the parameters corresponding to the selected coordinate or coordinate block; in the same iteration, other coordinates or coordinate blocks are fixed, and the overall objective function value and gradient are calculated for optimization. After the selected coordinates are optimized, the next coordinate or coordinate block is iterated. In the BCD method, a global multiparameter optimization problem can be divided into several single-parameter local optimization problems, and the optimal solution can be acquired by stepwise approximation (Wang et al., 2018; Zhao et al., 2015). Here, we introduce the BCD principle into the SA algorithm and propose the BCDSA algorithm.

The details of the BCDSA algorithm are as follows:

Input: Basic dispersion curve data, number of layers N_{layer}, Poisson's ratio σ, density ρ, initial temperature T_0, final temperature T_{end}, temperature drop coefficient α, maximum number of iterations num, and initial model m_0.

1: Initialize $m_0 = [Vs, Vp, h, \rho]$, and calculate the initial error E_0 by equation (1).

2. Divide the model m_0 into $2N_{layer}$ coordinate blocks, $m^i = [Vs^i, Vp, h, \rho](i \le n)$, or $m^i = [Vs, Vp, h^i, p](i > n)$.

3: **while** $T_0 > T_{end}$, **do**

4: for $i = 1, 2, \cdots, 2N_{layer}$, **do**

5: Perturb Vs^i according to equation (2) while keeping other parameters unchanged, and update Vp by equation (4) or perturb h^i with equation (2) while keeping the other parameters unchanged.

6: Calculate the error E_1 of the new model m_1 by equation (1), and accept the model m_1 if $E_1 < E_0$. Otherwise, accept m_1 with the probability $\exp(-(E_1 - E_0)/T_0)$. If m_1 is accepted, let $m_0 = m_1$ and $E_0 = E_1$.

7: **end for**

8: Update Vp with equation (4).

9: **end while**

Output: $m = m_0$.

2.4. Block coordinate descent differential evolution simulated annealing (BCDESA) algorithm

Although the BCDSA algorithm is suitable for the multiparameter, high-dimensional inversion of Rayleigh wave dispersion curves, this method does not directly control the decrease in error because it uses the temperature as the termination condition. Moreover, invalid disturbances under high temperatures may lead to insufficient disturbances, ultimately destabilizing the inversion results. Hence, we employ the diversity of population information in the DE algorithm (Storn and Price, 1997) to improve the stability of the BCDSA algorithm.

Here, the basic operations of the DE algorithm, namely, population initialization, mutation and recombination, are introduced.

2.4.1.1. Population initialization

An individual m_i is assumed to be in an N-dimensional matrix (i.e., a model with N layers) in population M, where Vs and h in m_i are

$$Vs^i = (Vs^i_1,\ Vs^i_2,\ \ldots,\ Vs^i_N), \tag{6a}$$

$$h^i = (h^i_1,\ h^i_2,\ \ldots,\ h^i_N). \tag{6b}$$

The first generation of the population is randomly generated as follows:

$$\begin{aligned} &Vs^i_j = rand(V_1, V_2), h^i_j = rand(H_1, H_2) \\ &i = 1, 2, \ldots, M, j = 1, 2, \ldots, N \end{aligned} \tag{7}$$

where rand(A, B) is a function to generate a random number ranging from A to B. Vp is updated according to equation (5), and ρ is constant. The final initialized population size is M, and the individual dimension is N.

2.4.1.2. Mutation

A new individual m_a can be mutated with two randomly selected individuals m_b and m_c:

$$m'_i(g+1) = m_a(g) + F(m_b(g) - m_c(g)) a \neq b \neq c, i = 1, 2, \ldots, M \tag{8}$$

where $m'_i(g+1)$ is the individual of the i^{th} variation in the $(g+1)^{th}$ generation; $m_a(g)$, $m_b(g)$, and $m_c(g)$ are three different individuals in the g^{th}-generation population; and $F \in [0, 2]$ is the scaling factor, for which 0.5 is used in this paper, where a large F results in a high diversity of the generated population and a small F leads to fast convergence (Rahnamayan et al., 2008). Vs and h are treated according to equation (8), and Vp is updated by equation (4), while the density remains unchanged.

2.4.1.3. Recombination

Taking Vs as an example, after the $(g+1)^{th}$ population mutation, the i^{th} individual $Vs_i(g+1)$ may recombine with the i^{th} individual $Vs_i(g)$ of the g^{th} population:

$$Vs^{j'}_i(g+1) = \begin{cases} Vs^j_i(g+1) r_i < CR \\ Vs^j_i(g) others \end{cases} i = 1, 2, \ldots, M, j = 1, 2, \ldots, N \tag{9}$$

where j represents the j^{th} dimension of $Vs^j_i(g+1)$ and $Vs^{j'}_i(g+1)$ is the result of recombination. r_i obeys a uniform distribution in (0,1). $CR \in [0, 1]$ is a recombination factor, which is usually much smaller than 1, such as 0.3 (Storn, 1996).

2.4.1.4. Selection

We use a greedy algorithm to select individuals in the next generation:

$$m_i(g+1) = \begin{cases} m'_i(g+1), E\left(m'_i(g+1)\right) < E(m_i(g)) \\ m_i(g), other \end{cases}, \tag{10}$$

The basic process of the DE algorithm is as follows:

1) Determine the control parameters of the DE algorithm, and determine the error function. The De algorithm control parameters include the population size NP, scaling factor F, and recombination factor CR.
2) Initialize the population according to equation (7).
3) If the population reaches the termination conditions, the best individual is the optimal solution; otherwise, the evolution needs to continue.
4) Obtain intermediate populations through mutation and recombination according to equations (8) and (9), respectively.
5) Select individuals from the original population and the intermediate population according to equation (10) to obtain a new generation of the population.
6) Advance the evolution generation number, i.e., $g = g + 1$, and go to step 3.

Generally, the SA algorithm is used for every individual in all populations, and the initial temperature is properly reduced to avoid invalid disturbances caused by high temperatures. The useful information of the parent can be inherited by the next generation, which can accelerate the convergence of the algorithm. Furthermore, the algorithm can directly control the decline in the error by replacing the traditional temperature termination condition with an error termination condition, which improves the stability of the algorithm and further increases the accuracy. The idea of using the error as the termination condition and utilizing population selection ensures the stability of the DE algorithm. Moreover, the richer the population information is, the more stable the algorithm. The detailed workflow of the proposed algorithm is shown in Fig. 1.

3. Performance analyses

We use two models to test the performance of BCDESA in the inversion of velocity profiles from Rayleigh wave dispersion curves. The models contain two and four layers with increasing velocity, as shown in Tables 1 and 2, respectively.

3.1. Performance of introducing BCD into SA

Although a higher-order mode was recently used (Wang et al., 2019), the mode most extensively applied during Rayleigh wave exploration is the fundamental-order Rayleigh wave because of its high energy and the ease with which it is observed (Yu et al., 2018). In this study, the dispersion curve of the fundamental-order Rayleigh wave is used to invert the near-surface Vs and h of each layer. Here, we use the improved fast generalized reflection-transmission coefficient method (Chen, 1993; Pei et al., 2008) to calculate the dispersion curves for different models.

During the inversion, the Vs and h in each layer usually range from 0.5 to 1.5 times the true value (Lu et al., 2016) to improve the accuracy. In practical applications, we can limit the search ranges of these two parameters based only on the Rayleigh wave dispersion curve because the phase velocity of the fundamental-order Rayleigh wave at the low-frequency limit is close to 0.92 times the Vs of the homogeneous half-space, and the corresponding high-frequency limit is close to 0.92 times the Vs of the first layer (Knopoff, 1964).

Moreover, the investigation depth of the Rayleigh wave is half of the maximum wavelength. We set the model range of Vs from the 0.5 times the minimum Rayleigh wave phase velocity to 1.5 times the maximum phase velocity. The layer thickness is greater than 0, and the sum of the layer thicknesses is smaller than the maximum wavelength.

We perform 10 inversions for the two models by both SA and BCDSA. The input parameters are the same for each inversion ($T0$, $Tend$, α), as listed in Table 3, and the Num is the iteration number required to meet the termination condition. The SA algorithm uses the alternating iterative optimization method for Vs and h (Pei et al., 2007). In the BCDSA

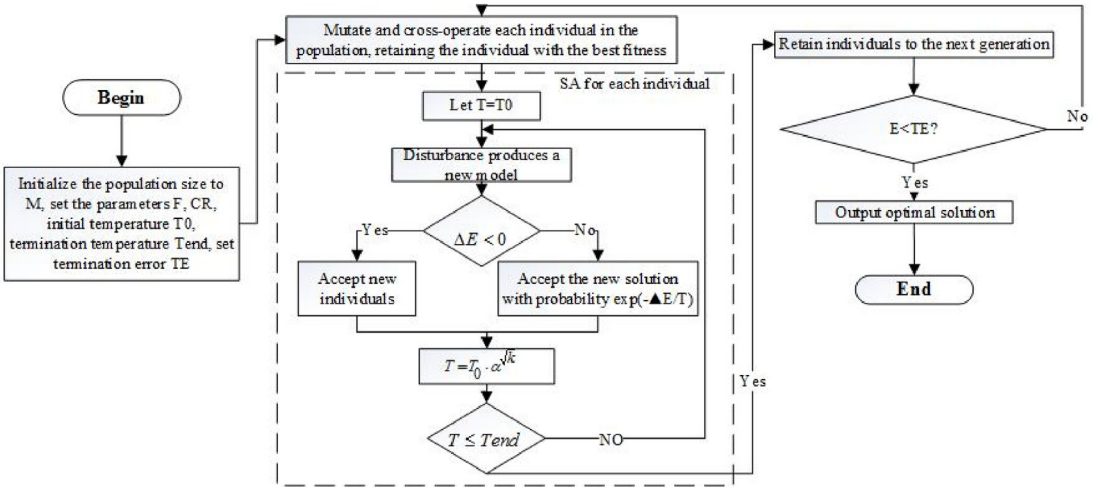

Fig. 1. The workflow of the BCDESA algorithm.

Table 1
Model A: Parameters of the two-layer model with increasing velocity.

Layer	*Vs* (m/s)	*Vp* (m/s)	ρ (kg/m^3)	*h* (m)
1	202	349.9	1900	5
2	301	521.3	1900	∞

Table 2
Model B: Parameters of the four-layer model with increasing velocity.

Layer	*Vs* (m/s)	*Vp* (m/s)	ρ (kg/m^3)	*h* (m)
1	201	348.1	1900	2
2	301	521.3	1900	4
3	403	698.0	1900	6
4	505	874.7	1900	∞

Table 3
Parameters of the SA and BCDSA algorithms. *T0*: initial temperature; *Tend*: termination temperature; *α*: temperature drop coefficient; *Num*: iteration number at the current temperature.

Parameters	Model A		Model B	
	SA	BCDSA	SA	BCDSA
T0	2000	2000	2000	2000
Tend	0.1	0.1	0.1	0.1
α	0.9	0.9	0.9	0.9
Num	40	20	200	50

algorithm, the number of coordinate blocks is set to 1; i.e., only one parameter is iterated at a time.

Fig. 2 shows the error distributions of ten tests. The errors of the results obtained by the SA method may suddenly change (the errors of the two results in Fig. 2a are abnormally large), whereas the errors of the BCDSA method are stable. The average error and variance in the 10 inversions for Models A and B, respectively (see Table 4) illustrate that the introduction of the BCD method into the SA algorithm can significantly improve the accuracy of the latter, especially when the number of model layers increases.

The smallest *Vs* errors are obtained for Models A and B among the 10 inversion tests, and the forward modeling dispersion curves are shown in Figs. 3 and 4. The maximum relative error of *Vs* in Model A is 1.85% and 0.62% for the SA and BCDSA inversion, respectively, and the relative error of *h* is 9.31% and 1.22%, respectively. With increasing depth (Model B), the BCDSA inversion results are significantly better than SA results. Table 5 lists the inversion results and errors for Model B. The BCDSA inversion results for each layer are better than the SA results. In particular, BCDSA greatly improves the inversion accuracy with increasing depth. Fig. 5 shows the decreasing trend of errors during the inversion by using SA and BCDSA. The overall error of the BCDSA algorithm exhibits a decreasing trend with decreasing temperature, which indicates that BCDSA has the capability to jump out of local optima, but the SA method cannot (iteration>680 in Fig. 5a and iteration>2600 in Fig. 5b).

3.2. Performance of the introduction of DE into the BCDSA (BCDESA)

Because BCDSA uses the temperature as a termination condition, the inversion commonly terminates even if the error does not achieve the requirement when the temperature reaches 0 (Table 4). In addition, SA and BCDSA are particularly susceptible to accepting a worse solution due to the limitation of the Metropolis criterion when the number of iterations is relatively small (i.e., at higher temperatures, see Fig. 5). Consequently, it is easy to obtain invalid results in unsatisfactory inversions. In general, BCDSA cannot control the error direction. One solution is to use the DE algorithm to control the termination error by replacing the temperature termination condition with an error termination condition. The workflow of the BCDESA method is shown in Fig. 1.

We use Model B as an example to test the performance of BCDESA. The parameters for the BCDESA inversion are as follows: population size $M = 10$, scaling factor $F = 0.5$, crossover factor $CR = 0.3$, initial temperature $T0 = 25$, termination temperature $Tend = 0.1$, temperature drop coefficient $\alpha = 0.8$, and current temperature maximum iteration number $Num = 2$. We set the initial temperature as 25 in BCDESA because the BCDSA algorithm still has a strong ability to jump out of local solutions when the temperature is between 28 and 18 °C (Iteration>650 in Fig. 5a and Iteration>3300 in Fig. 5b). In addition, the relatively low initial temperature also reduces the computational time.

To illustrate the controllability of the BCDESA error, we test two cases where the termination error *E* is 4.5 and 2.0. The other parameters are constant in the inversions. Fig. 6 shows a comparison between the outcomes of the two inversion tests, and Table 6 lists the inversion results for each layer. Compared with the BCDSA inversion accuracy (Table 5), the BCDESA inversion accuracy is higher. However, a lower inversion error requires more iterations, resulting in an increased number of calculations (Fig. 7).

4. Synthetic data examples

In this section, we test the performance of the BCDESA inversion method with 3 typical layered models (Pei et al., 2007): Models C

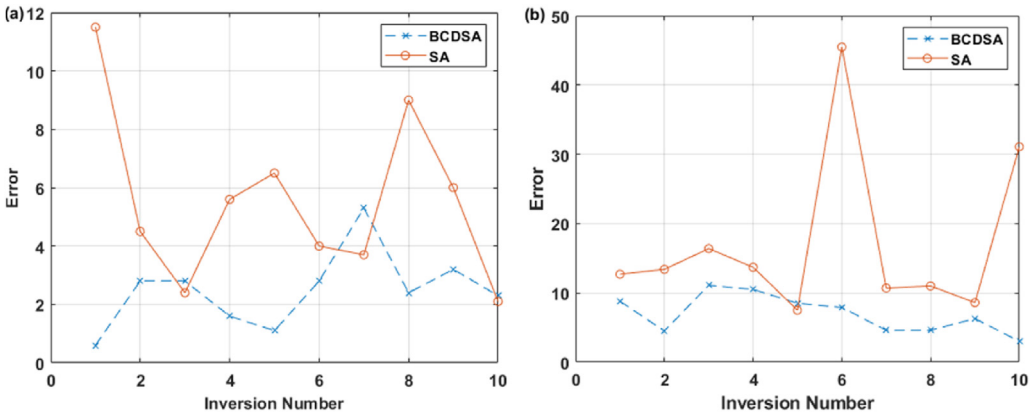

Fig. 2. Error distribution for 10 inversions using different methods. (a) Model A; (b) Model B. The error is calculated by equation (1). The blue points are the BCDSA errors, and the black crosses are the SA errors. The BCDSA error is lower than the SA error. In Model B, SA has two large error anomalies.

Table 4
Stability analysis of the inversion errors from ten tests by using SA and BCDSA for two models (the error is calculated by equation (1)).

	Model A		Model B	
	SA	BCDSA	SA	BCDSA
Mean error	5.69	2.73	17.06	6.98
Variance	8.18	2.54	143.36	7.74

(Table 7), D (Table 8), and E (Table 9). The *Vs* of each layer in Model C is increasing, while Model D contains a high *Vs* interlayer, and Model E has a low *Vs* interlayer.

The computation time is also affected by the population size *M*, which is usually a multiple of 10 (Storn, 1996). We use **Model B** as an example to test the influence of the population size *M* on the BCDESA algorithm. *M* is set as 10, 20, and 30, and the termination error is set as 4.5. The other parameters are the same as those in Fig. 6. Table 10 lists the average algebra of generations for the convergence (CAA) and average number of individuals generated(ANI) of the algorithm. A value of 10 is the best choice for *M* because this value is the minimum number of generations, which requires the fewest computations.

4.1. Noiseless case

Here, we use the BCDESA and SA methods to invert the 3 typical models without any noise. The parameters for the BCDESA inversion are the same as those in Fig. 6, except the termination error is 4.5. The parameters for the SA inversion are the same as in Model B in Table 3. Figs. 8–10 show comparisons between the models and inversion results. Figs. 8–10(a) show comparisons between the true model dispersion curve (red solid curve) and the forward modeling inversion curves (blue curve for BCDESA and black dotted curve for SA). Similarly, Figs. 8–10(b) show comparisons between the *Vs* profile of the true model (red curve) and the inverted profiles (blue curve for BCDESA and gray curve for SA). The dispersion curves obtained by BCDESA are closer to the true dispersion curve, but SA cannot obtain a good result, especially for Model D (Fig. 9b), where *Vs* and *h* considerably deviate from the model values. The maximum errors of the inverted *Vs* for Models C, D, and E from

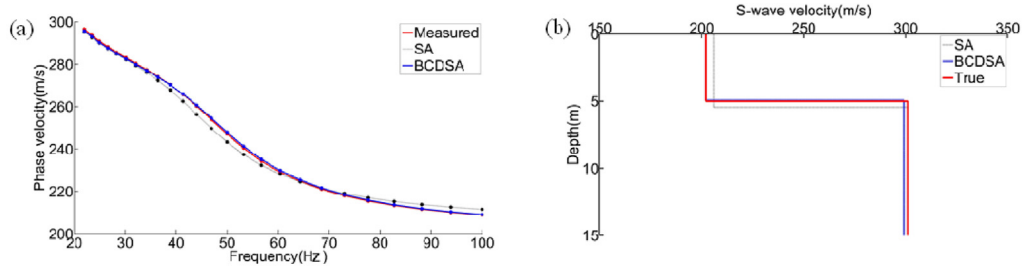

Fig. 3. Inversion results of SA and BCDSA for Model A. (a) shows the dispersion curve. The red line is the true dispersion curve of Model A, and the blue and black lines are obtained from the inversion results of BCDSA and SA, respectively. (b) shows the Vs profile. The red line is the true value of Model A, and the blue and black lines are the inversion results of BCDSA and SA, respectively.

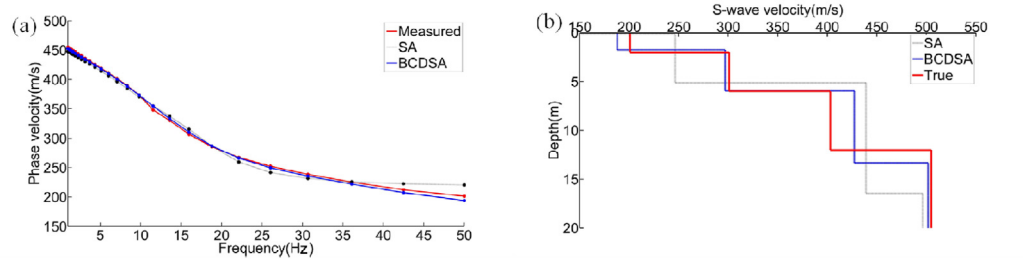

Fig. 4. SA and BCDSA inversion results for Model B. The representations of the lines are the same as in Fig. 3.

Table 5
Statistics of the inversion results for Model B (RE stands for relative error).

Parameters	True values	SA			BCDSA		
		Inverted	RE (%)	MSE	Inverted	RE (%)	MSE
V1 (m/s)	201	137.5	31.57	7.5	187.9	6.50	3.0
V2 (m/s)	301	246.4	18.14		296.7	1.41	
V3 (m/s)	403	439.0	8.93		427.3	6.02	
V4 (m/s)	505	496.2	1.74		501.7	0.65	
H1	2	0.13	93.35		1.76	11.93	
H2	4	4.98	24.47		4.19	4.66	
H3	6	11.36	89.25		7.39	23.09	

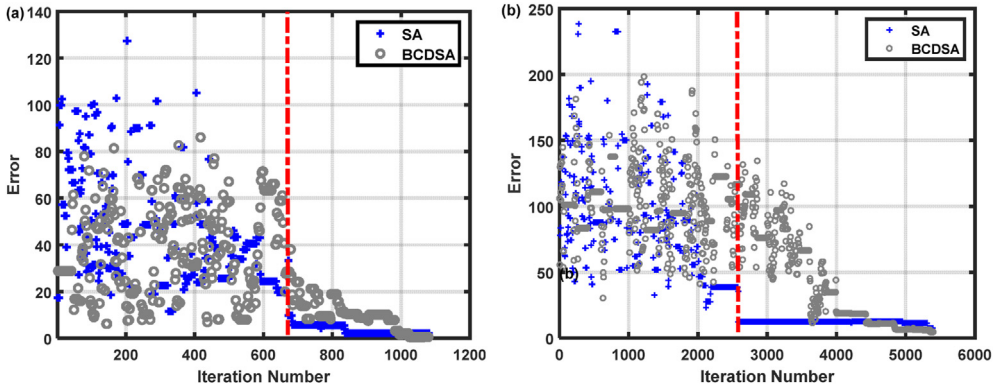

Fig. 5. Variations in the errors with increasing iterations. (a) is Model A, and (b) is Model B. The error is calculated by equation (1). Although SA converges faster than BCDSA when the iteration number is small, BCDSA still has the potential to jump out of local solutions as the iteration number increases, enabling BCDSA to obtain a better solution.

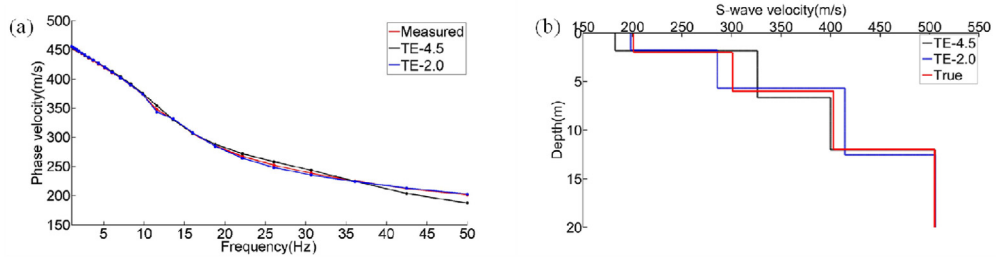

Fig. 6. BCDESA inversion of Model B under different termination errors. (a) shows the dispersion curves; (b) shows the *Vs* profiles. The black, blue, and red curves are the inversion results with the termination error set to 4.5, 2.0, and the true value, respectively.

BCDESA are 2.55%, 3.64% and 5.14%, respectively, while the errors from SA are 3.15%, 24.38% and 13.64%, respectively. The maximum errors of *h* are 6.45%, 5.60% and 12.40% in the BCDESA inversion, while the corresponding *h* errors are 8.80%, 22.47% and 33.67% in the SA inversion, respectively.

Table 6
Statistics of the inversion results for Model B for different TEs. TE and RE represent the termination error and relative error, respectively.

Parameters	True value	Termination error = 4.5			Termination error = 2.0		
		Inverted	RE (%)	MSE	Inverted	RE (%)	MSE
V1 (m/s)	201	182.4	9.27	4.1	198.5	1.27	1.8
V2 (m/s)	301	326.1	8.33		285.5	5.14	
V3 (m/s)	403	400.1	0.73		414.6	2.87	
V4 (m/s)	505	505.5	0.09		506.1	0.21	
H1	2	1.84	8.15		1.79	10.51	
H2	4	4.82	20.42		3.88	2.94	
H3	6	5.37	10.47		6.88	14.67	

4.2. Noisy case

In field applications, recorded seismic data inevitably contain noise, which may reduce the accuracy and stability of the inversion algorithm.

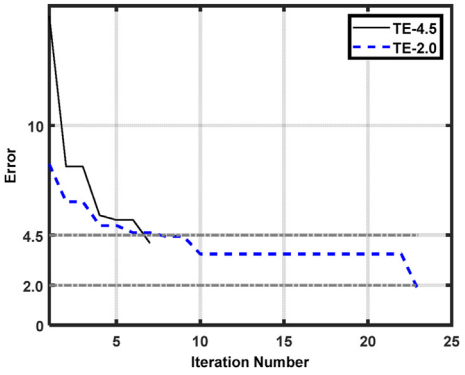

Fig. 7. Variation in the error with the number of iterations. The generations significantly increase if the termination error is small.

Table 7
Parameters for Model C: an increasing Vs layer model.

Layer number	S-wave velocity (m/s)	P-wave velocity (m/s)	Density (kg/m^3)	Thickness (m)
1	380	658.2	2000	10
2	540	935.3	2000	25
3	700	1056.6	2000	∞

Table 8
Parameters for Model D: a high-Vs interlayer model.

Layer number	S-wave velocity (m/s)	P-wave velocity (m/s)	Density (kg/m^3)	Thickness (m)
1	900	1558.8	2000	28
2	1340	2338.3	2000	24
3	1200	2078.5	2000	∞

Table 9
Parameters for Model E: a low-Vs interlayer model.

Layer number	S-wave velocity (m/s)	P-wave velocity (m/s)	Density (kg/m^3)	Thickness (m)
1	510	883.3	2000	10
2	400	692.8	2000	16
3	700	1212.4	2000	∞

Table 10
Convergence comparison of BCDESA with various values of the population size M.CAA is the convergent average generation. ANI is the average individual number, which represents the number of calculations.

M	10	20	30
CAA	2.16	1.92	1.91
ANI	21.	38.4	57.4

We add Gaussian noise of 20 dB to the dispersion curve to test the performance of the BCDESA and SA algorithm under noisy conditions. We set the termination error of the BCDESA to 12 because the mean square error (E) of the noisy data and the clean data is between 10 and 11. The other parameters are not changed.

Figs. 11–13 show comparisons between the model and the inversion results for Models C, D, and E, respectively. In Figs. 11–13(a), the red curves are the dispersion curves of the models with added noise. The blue and black dotted curves are the dispersion curves from the inversion results. Similarly, Figs. 11–13(b) show comparisons of the *Vs* profiles between the true model (red curve) and the inverted models (blue curve for BCDESA and gray curve for SA). The maximum errors of the inverted *Vs* from BCDESA for Models C and D, E are 5.43%, 6.01% and 5.14%, respectively, while the errors from SA are 9.14%, 9.81% and 9.79%, respectively. The maximum errors of the inverted *h* are 3.10%, 7.12% and 12.39% in BCDESA, while the corresponding errors are 55.10%, 9.27% and 24.39% in the SA inversion, respectively. The comparable results between the noise-free and noisy data illustrate the good performance of the BCDESA algorithm.

5. Field data example

To further test the applicability of BCDESA, we employ the BCDESA method to invert the near-surface structure by using field data acquired in southwestern China. Fig. 14 shows the acquisition system: the GTDS-10H seismometers are arranged with a minimum source-receiver spacing of 1 m and a receiver interval of 2 m; the time interval is 1 ms, and the record length is 2 s. Fig. 15a shows the array waveform recordings. The energy is concentrated mainly between the 70th and 170th traces. A dispersion analysis (Fig. 16b) is conducted by applying an *F–K* transform to the waveforms in channels 121–168. Within the frequency range of 10–30 Hz, we can see more than one mode in Fig. 16b. Here, we manually pick only the dispersion curve of the fundamental mode (see the dotted curve in Fig. 15b) to invert the near-surface velocity profile.

Core samples were collected approximately 40 m from the research area, and the lithological column is shown in Fig. 16a. Table 11 lists the *h* and *Vs* of each layer. Fig. 16b shows the inverted results from BCDESA

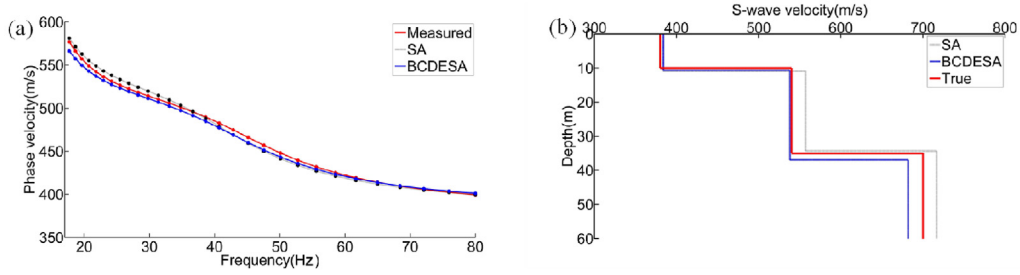

Fig. 8. Inversion results and synthetic dispersion curves of Model C from BCDESA and SA. (a) is a comparison between the true model dispersion curve (red solid curve) and the best matching dispersion curves from the inversion (blue curve for BCDESA and black dotted curve for SA). (b) is a comparison between the *Vs* profile of the true model (red curve) and the inverted profiles (blue curve for BCDESA and gray curve for SA).

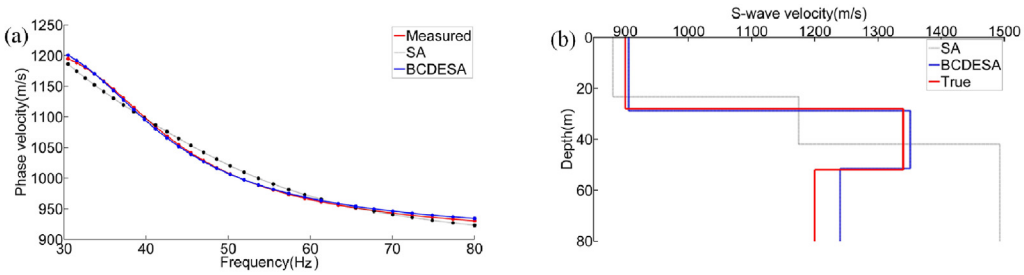

Fig. 9. Inversion results and the synthetic dispersion curves of Model D from BCDESA and SA. The description of the figure is the same as in Fig. 8.

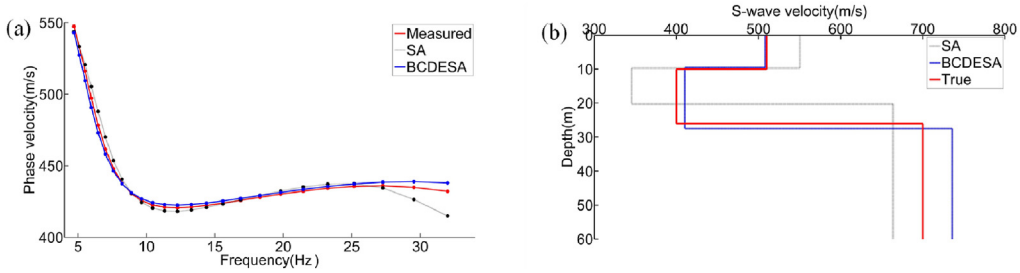

Fig. 10. Inversion results and the synthetic dispersion curves of Model E from BCDESA and SA. The description of the figure is the same as in Fig. 8.

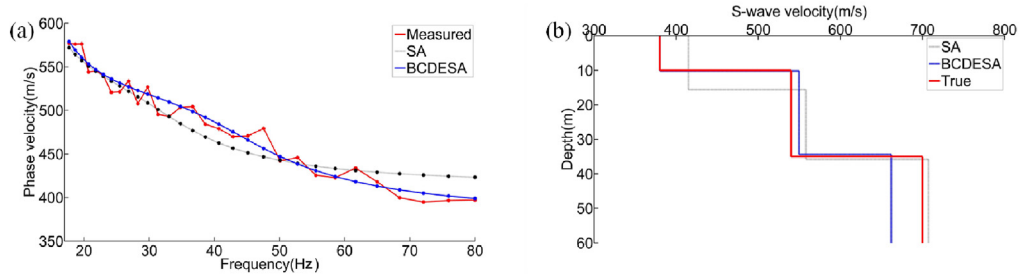

Fig. 11. Inversion results for Model C from the noise-added (20 dB) dispersion curve of Model C. The description of the figure is the same as in Fig. 8.

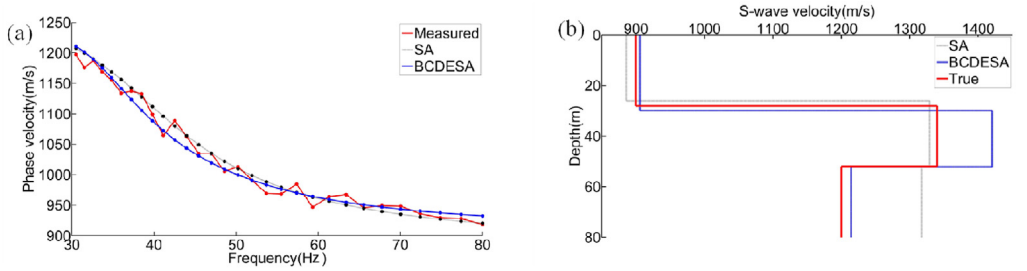

Fig. 12. Invert results of Model D from the noise-added (20 dB) dispersion curve of Model C. The description of the figure is the same as in Fig. 8.

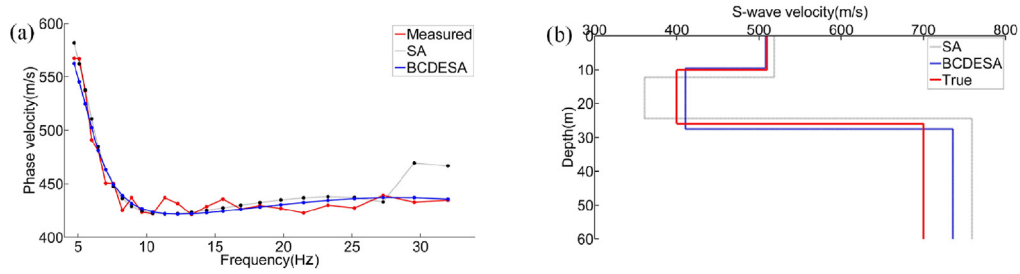

Fig. 13. Invert results of Model E from the noise-added (20 dB) dispersion curve of Model C. The description of the figure is the same as in Fig. 8.

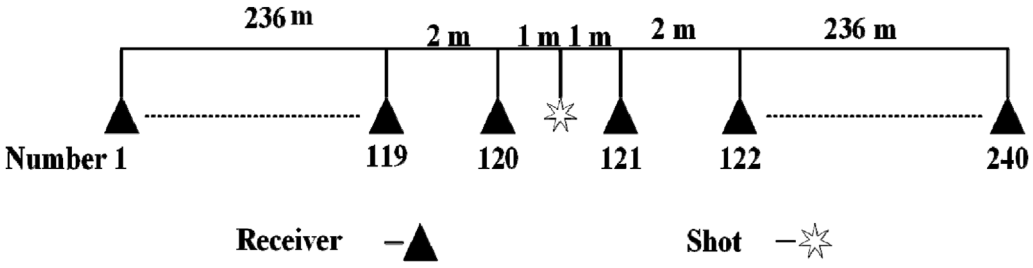

Fig. 14. Schematic diagram of the acquisition system. A portable vibroseis source is used.

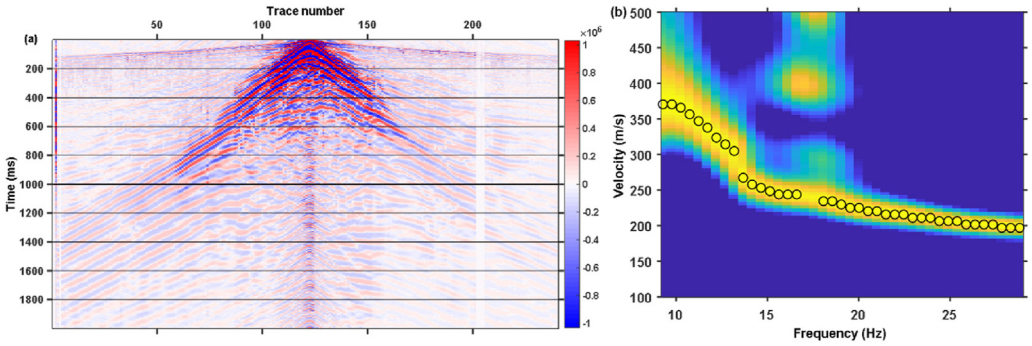

Fig. 15. (a) Array waveform recordings. (b) is the *F–K* spectrum of the waveforms from channels 121–168 in (a). The dotted curve is the manually picked dispersion curve of the fundamental Rayleigh mode.

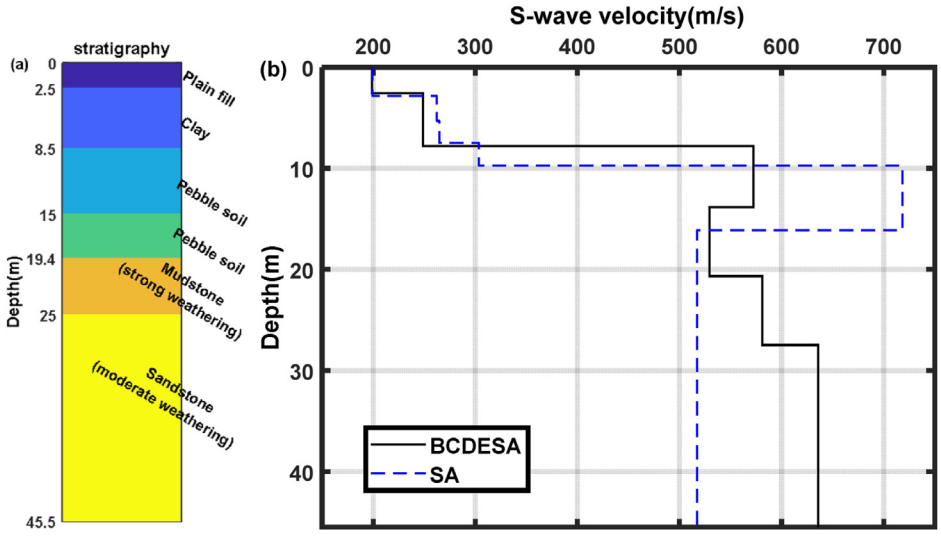

Fig. 16. (a) Lithological profile from core samples; **(b)** *Vs* profile obtained by the inversion.

Table 11
Lithology and Vs information from the core samples.

Starting depth (m)	Final depth (m)	Lithology	S-wave velocity range (m/s)
0	2.5	Plain fill	200~300
2.5	8.5	Clay	180~300
8.5	15	Pebble soil	300~600
15	19.4	Pebble soil	300~600
19.4	25	Mudstone (strong weathering)	600~1300
25	45.5	Sandstone (moderate weathering)	600~1300

(gray curve) and SA (blue curve). In this inversion, the number of layers is set as 6 in the SA inversion, and the search range of the total thickness is from 10 m to 30 m. The search range of *Vs* is from 0.5 times the minimum phase velocity to twice the maximum phase velocity. The other parameters are the same as the parameter settings in Model B (Table 3). The parameters in BCDESA, such as the number of layers and the search ranges of the total thickness and *Vs*, are the same as those in the SA inversion. Although the search range of *Vs* is the same, the initial model *Vs* is not known in advance in the BCDESA inversion.

Fig. 17 shows the dispersion curves from the inverted models (blue curve for BCDESA and black curve for SA) and the dispersion curve extracted from the measured waveform (red curve). The dispersion curve from the model inverted by the BCDESA method has relatively small errors at low frequencies. Quantitative analysis reveals that the errors of

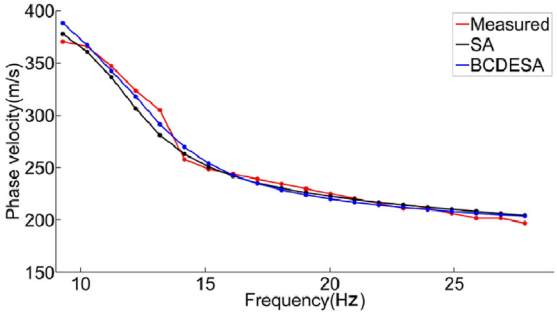

Fig. 17. Forward modeling dispersion curves from the inversions. The blue curve is the result from BCDESA, and the black curve is the result from SA. The red curve represents the dispersion curve extracted from the observed seismic waveform.

the *Vs* profiles from the BCDESA and SA methods are 6.67 and 7.85, respectively, which further illustrates the effectiveness of the BCDESA method. To verify the accuracy of BCDESA, we use the X^2 test, which is defined as:

$$X^2 = \sum_{i=1}^{k} \frac{(o_i - e_i)^2}{e_i} \tag{11}$$

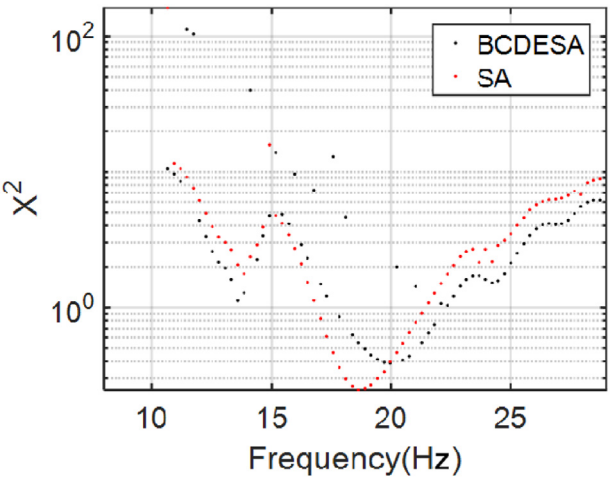

Fig. 18. Results of X^2 test. The blue points are the results from BCDESA, and the red points are the results from SA.

Table 12
Inversion results of the BCDESA and SA algorithms.

BCDESA		SA	
Layer thickness (m)	*Vs* (m/s)	Layer thickness (m)	*Vs* (m/s)
2.56	199.0	2.82	199.3
5.21	249.2	2.49	262.2
6.06	572.5	2.15	264.8
6.83	529.4	2.27	303.6
6.80	581.0	6.39	718.4
∞	635.9	∞	517.2

where o_i is the observed dispersion curve, e_i is the dispersion curve forward modeling of *Vs* obtained by inversion, and k represents k number inversion are carried out. The results of X^2 obtained by the above equation is expressed as a sort of normalized distance between observed and the synthesized data. As can be seen from Fig. 18, BCDESA has a smaller deviation than SA from the statistics. Table 12 lists the results from the BCDESA and SA inversions in detail. The inversion results from the BCDESA method closely follow the borehole lithology, indicating that the BCDESA method is more accurate than the SA method alone.

6. Conclusion

The inversion of *Vs* profiles from Rayleigh wave dispersion curves constitutes a typical nonlinear inverse problem, which is characterized by multiple inversion parameters and high dimensionality. It is not easy to solve such a problem by using a traditional nonlinear inversion technique, such as the SA algorithm, because an increase in the number of layers (a random iterative direction) leads to large errors in high-dimensional nonlinear problems. Based on the SA algorithm, we propose the BCDESA algorithm, where the high-dimensional nonlinear SA parameter inverse problem is solved by the BCD algorithm. By using the population evolution and optimal control attributes of the DE technique, the SA algorithm is transformed to control the whole iterative process with error, thereby avoiding the instability of the inversion algorithm. This method can also be used to solve other nonlinear inverse problems in the future.

In this study, we systematically verify the feasibility of the proposed method through experimental analysis. First, the BCD method is used to improve the SA algorithm, which divides the high-dimensional parameter inverse problem of Rayleigh waves into several single-parameter low-dimensional inverse problems and makes full use of the strong SA solution to the single-parameter low-dimensional problem to improve the SA inversion accuracy. From two model experiments with different sets of layer thicknesses, compared to that of the SA algorithm, the accuracy of the BCDSA algorithm after introducing the principle of BCD is effectively improved, especially when the number of layers is increased, and the improvement effect is more obvious. Furthermore, comparative experiments reveal that for both BCDSA and SA, local optimization will occur during the iteration process, and controlling the iteration by a temperature control alone may cause unstable results. In view of the above problems, this paper further introduces the DE algorithm and changes the termination condition of the BCDSA algorithm from a temperature condition to an error condition. This modification realizes the control of the whole iterative process by using the abovementioned error and ultimately improves the stability of the algorithm. Finally, we use three typical theoretical models to show that the BCDESA algorithm has a better inversion accuracy than the SA algorithm, especially in the inversion of low-speed interlayers, and can identify high-speed interlayers. Moreover, the inversion of actual data in western China show that the inversion results of the BCDESA algorithm are consistent with drilling data, while the SA algorithm has a large deviation.

In the experiment, we also find that the proposed method can set the Vs and depth ranges automatically according to the Rayleigh wave velocity and wavelength, which can achieve accurate and reliable inversion results while avoiding the problem of the traditional method, which needs to set the ranges of the inversion parameters artificially. This provides convenience for practical applications and enables the industrialization of the proposed method.

Declaration of competing interest

The authors declare that they have no known competing financial interests or personal relationships that could have appeared to influence the work reported in this paper.

Acknowledgements

This study is supported by National Natural Science Foundation of China (NOs. 41974150, 42174158, 42174151, 41804126), a supporting program for outstanding talent of the University of Electronic Science and Technology of China (No. 2019-QR-01), and Project of Basic Scientific Research Operating Expenses of Central Universities (ZYGX2019J071; ZYGX 2020J013). We thank three anonymous reviewers whose comments substantially improved the presentation of our work.

References

Beaty, K.S., Schmitt, D.R., Sacchi, M., 2002. Simulated annealing inversion of multimode Rayleigh wave dispersion curves for geological structure. Geophys. J. Int. 151, 622–631.
Chen, X., 1993. A systematic and efficient method of computing normal modes for multilayered half-space. Geophys. J. Int. 115, 391–409.
Dal Moro, G., Pipan, M., Gabrielli, P., 2007. Rayleigh wave dispersion curve inversion via genetic algorithms and marginal posterior probability density estimation. J. Appl. Geophys. 61, 39–55.
Foti, S., Parolai, S., Albarello, D., Picozzi, M., 2011. Application of surface-wave methods for seismic site characterization. Surv. Geophys. 32, 777–825.
Ingber, L., 1989. Very fast simulated Re-annealing. Math. Comput. Model. 12, 967–973.
Kirkpatrick, S., Gelatt, C.D., Vecchi, M.P., 1983. Optimization by simulated annealing. Science 220, 671–680.
Knopoff, L., 1964. A matrix method for elastic wave problems. B SEISMOL SOC AM 54, 431–438.
Lu, Y., Peng, S., Du, W., Zhang, X., Ma, Z., Lin, P., 2016. Rayleigh wave inversion using heat-bath simulated annealing algorithm. J. Appl. Geophys. 134, 267–280.
Park, C.B., Miller, R.D., Xia, J., 1999. Multichannel analysis of surface waves. Geophysics 64, 800–808.
Pei, D., Louie, J.N., Pullammanappallil, S.K., 2007. Application of simulated annealing inversion on high-frequency fundamental-mode Rayleigh wave dispersion curves. Geophysics 72, R77–R85.
Pei, D., Louie, J.N., Pullammanappallil, S.K., 2008. Improvements on computation of phase velocities of Rayleigh waves based on the generalized R/T coefficient method. B SEISMOL SOC AM 98, 280–287.
Pugin, A.J.M., Pullan, S.E., Hunter, J.A., 2013. Shear-wave high-resolution seismic reflection in Ottawa and Quebec city, Canada. Lead. Edge 32, 250–255.

Qi, S., Sun, J., He, H., 2002. Review of Rayleigh wave exploration. Prog. Geophys. 17 (4), 630–635.
Rahnamayan, S., Tizhoosh, H.R., Salama, M.M., 2008. Opposition-based differential evolution. IEEE T EVOLUT COMPUT 12, 64–79.
Ryden, N., Park, C.B., 2006. Fast simulated annealing inversion of surface waves on pavement using phase-velocity spectra. Geophysics 71, R49–R58 s.
Storn, R., 1996. On the usage of differential evolution for function optimization. In: Proceedings of North American Fuzzy Information Processing, pp. 519–523IEEE.
Storn, R., Price, K., 1997. Differential evolution–A simple and efficient heuristic for global optimization over continuous spaces. J. Global Optim. 11, 341–359.
Wang, J., Wu, G., Chen, X., 2019. Frequency-bessel transform method for effective imaging of higher-mode Rayleigh dispersion curves from ambient seismic noise data. J. Geophys. Res.: Solid Earth 124 (4), 3708–3723.
Wang, Y., Lin, W., Cheng, S., She, B., Hu, G., Liu, W., 2018. Sharp and laterally constrained multitrace impedance inversion based on blocky coordinate descent. Acta Geophys. 66, 623–631.
Xia, J., Miller, R.D., Park, C.B., 1999. Estimation of near-surface shear-wave velocity by inversion of Rayleigh waves. Geophysics 64, 691–700.
Xu, Y., Yin, W., 2015. A block coordinate descent method for regularized multiconvex optimization with applications to nonnegative tensor factorization and completion. SIAM J IMAGING SCI 6, 1758–1789.
Xia, J., Gao, L., Pan, Y., Shen, C., Yin, X., 2015. New findings in high-frequency surface wave method. Chin. J. Geophys. 58 (8), 2591–2605.
Yu, D., Song, X., Jiang, D., Zhang, X., Zhao, S., Zhao, P., Cai, W., Yuan, S., 2018. Improvement of artificial bee colony and its application in Rayleigh wave inversion. Chin. J. Geophys. 61 (4), 1482–1495.
Zhang, H., Maceira, M., Roux, P., Thurber, C., 2014. Joint inversion of body-wave arrival times and surface-wave dispersion for three-dimensional seismic structure around SAFOD. Pure Appl. Geophys. 171, 3013–3022.
Zhao, Q., Meng, D., Xu, Z., Gao, C., 2015. A block coordinate descent approach for sparse principal component analysis. Neurocomputing 153, 180–190.